Magnetic Resonance in Medicine 62:468–475 (2009)

High Resolution Diffusion-Weighted Imaging Using Readout-Segmented Echo-Planar Imaging, Parallel Imaging and a Two-Dimensional Navigator-Based Reacquisition

David A. Porter,[1*] and Robin M. Heidemann[2]

Single-shot echo-planar imaging (EPI) is well established as the method of choice for clinical, diffusion-weighted imaging with MRI because of its low sensitivity to the motion-induced phase errors that occur during diffusion sensitization of the MR signal. However, the method is prone to artifacts due to susceptibility changes at tissue interfaces and has a limited spatial resolution. The introduction of parallel imaging techniques, such as GRAPPA (GeneRalized Autocalibrating Partially Parallel Acquisitions), has reduced these problems, but there are still significant limitations, particularly at higher field strengths, such as 3 Tesla (T), which are increasingly being used for routine clinical imaging. This study describes how the combination of readout-segmented EPI and parallel imaging can be used to address these issues by generating high-resolution, diffusion-weighted images at 1.5T and 3T with a significant reduction in susceptibility artifact compared with the single-shot case. The technique uses data from a 2D navigator acquisition to perform a nonlinear phase correction and to control the real-time reacquisition of unusable data that cannot be corrected. Measurements on healthy volunteers demonstrate that this approach provides a robust correction for motion-induced phase artifact and allows scan times that are suitable for routine clinical application. Magn Reson Med 62:468–475, 2009. © 2009 Wiley-Liss, Inc.

Key words: readout-segmented EPI; parallel imaging; GRAPPA; 2D navigator; diffusion weighted imaging

The application of diffusion-weighted imaging in clinical studies is well established, particularly in the evaluation of acute stroke (1–3). These studies typically rely on single-shot diffusion-weighted echo-planar imaging (EPI; 4) which provides reliable clinical images free from motion-induced artifact. However, as is well documented, single-shot EPI is sensitive to susceptibility artifacts at tissue interfaces and suffers from a limitation to the maximum resolution that can be achieved. Although the introduction of parallel imaging techniques to single-shot acquisition methods like EPI (5–8) has reduced these effects, there are still significant residual problems. This is particularly true at higher field strengths where there is an increased level of susceptibility artifacts and increased blurring due to a shorter T_2^* relaxation time. The effect of field strength is a significant consideration because of the increasing amount of routine clinical imaging that is being performed at field strengths of 3 Tesla (T) and above.

Motion during the diffusion-sensitizing gradients leads to a spatially dependent phase variation that is different from one excitation to the next. This produces a very high level of artifact if standard multishot imaging techniques are used. In the case of rigid body motion, this phase variation is a linear function of position (9,10). However, the effect of cerebrospinal fluid (CSF) pulsation on the brain is to induce deformations, which do not conform to a rigid-body model. In this case, the resulting phase variation has a more general nonlinear behavior in two dimensions (11).

To compensate for this phase variation, navigator echo acquisitions were introduced into multishot sequences to monitor the shot-to-shot phase changes and apply a suitable correction to the data (9,10). Initial implementations, based on spin-echo sequences, used an additional echo to reacquire the central line of *k*-space at each excitation and applied a linear phase correction along the readout direction. Subsequently, the technique was extended to use 2D navigators to perform linear phase correction in both readout and phase-encoding directions in interleaved segmented EPI acquisitions (12,13).

More recently, alternative sequence types and modified phase-correction techniques have made it possible to apply a nonlinear, 2D phase-correction using navigator data. This is an essential requirement to achieve a robust correction for the phase errors that occur in diffusion-weighted imaging of the brain. This type of correction typically involves transforming to the image domain and performing a complex multiplication of the imaging signals with data derived from the corresponding 2D navigator. It is also possible to apply an equivalent correction using a direct deconvolution of the *k*-space data (11). As only a subset of *k*-space points are sampled at each excitation, the image domain data used in this process do not provide an accurate representation of the actual 2D spatial variation of signal. In particular, *k*-space sampling strategies that do not fulfill the Nyquist condition for the required field of view (FOV) at each shot result in aliasing, which complicates the image-domain 2D phase correction. Promising results have been shown using iterative phase correction algorithms to address the problem of aliasing in several sequences, including true FISP (11), spiral imaging (14), and interleaved EPI (15). However, these techniques

[1]Siemens AG, Healthcare Sector, Erlangen, Germany.

[2]Max Planck Institute for Human Cognitive and Brain Sciences, Department of Neurophysics, Leipzig, Germany.

*Correspondence to: David A. Porter, Siemens AG, Healthcare Sector, MED MR PLM AW Neurology, Allee am Roethelheimpark 2, 91052 Erlangen, Germany. E-mail: david.a.porter@siemens.com

Received 25 August 2008; revised 19 February 2009; accepted 25 February 2009.

DOI 10.1002/mrm.22024

Published online 15 May 2009 in Wiley InterScience (www.interscience.wiley.com).

require intensive computation and may not always provide a robust estimate for the required phase correction.

The image-domain 2D nonlinear phase correction is much less challenging when acquisition schemes are used that fulfill the Nyquist condition by sampling a contiguous set of *k*-space points at each excitation. In this case, an unaliased image can be reconstructed from the data from each shot and the phase correction can be applied as a noniterative complex multiplication. One sequence that fulfils this condition is diffusion-weighted PROPELLER (16), which uses a train of spin echoes to sample a band of contiguous *k*-space sample points, centered at the *k*-space origin. At each shot, the orientation of the band is varied to provide complete *k*-space coverage. The spin echo train makes the method insensitive to susceptibility-based distortion, but introduces the possibility of artifacts relating to the failure of the CPMG condition (Carr-Purcell-Meiboom-Gill) due to motion-induced phase shifts during the diffusion preparation (17). This problem is more severe at higher fields due to a greater deviation in refocusing pulse angle from 180 degrees due to the increased B_1 field variation. An alternative variant of PROPELLER avoids the CPMG issue by using an EPI echo-train to acquire the blades (18), but is sensitive to blurring related to T_2^* decay and off resonance effects.

Another sequence, which meets the Nyquist sampling condition at each shot, is diffusion-weighted, readout-segmented EPI (19), which can be modified to acquire a 2D navigator echo for nonlinear phase correction (20). This technique uses a much shorter echo-spacing than single-shot EPI, thereby reducing susceptibility and T_2^* blurring artifacts. The sequence uses a Cartesian *k*-space sampling scheme, resulting in fewer spin excitations and a shorter scan time than a corresponding PROPELLER sequence.

Although 2D navigator correction is usually effective at removing the shot-to-shot nonlinear phase variation in multishot diffusion-weighted imaging, the correction fails for severely corrupted data sets, in which signal voids occur in the navigator images. These signal voids correspond to a shift of low spatial-frequency components outside of the *k*-space acquisition window used for the navigator. In these cases, a complete correction of the data is not possible. Although this is an infrequent problem, it is essential that the issue is addressed to provide a robust technique that can be used with confidence in clinical studies. One way to deal with the problem is to use cardiac gating to avoid acquiring data from the affected slices during the systolic part of the cardiac cycle, which corresponds to the highest level of CSF pulsation and related brain deformation (21,22). In addition to the loss of efficiency compared with ungated acquisitions, this approach to the problem has additional practical disadvantages, including variability in repetition time (TR) and interval between heartbeats. As an alternative, some multishot techniques address the problem of uncorrectable data sets by simply omitting these data from the reconstruction (16). This is obviously only an option if there is sufficient redundancy in the sampling scheme for data from some shots to be discarded without severely degrading the final image.

A more elegant and efficient approach to the problem of uncorrectable data is to reacquire the unusable data as part of the acquisition process. Previous work with 1D navigators demonstrated that an appropriate reacquisition scheme can substantially reduce artifacts in diffusion-weighted spin-echo images, while limiting the additional scan time required for the reacquisition (23,24).

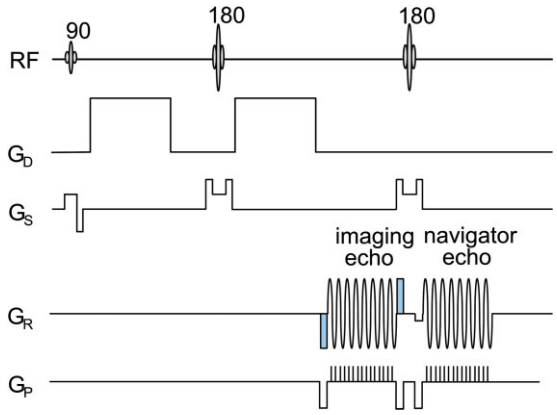

FIG. 1. Sequence diagram for a single readout segment: Following a diffusion preparation (G_D), two spin echoes are used to sample imaging and navigator echo. For the first spin echo a variable amplitude prephasing gradient pulse (colored blue) is applied to define an offset along k_x, which varies from shot to shot to sample a different segment in *k*-space. For the second echo a constant amplitude prephasing gradient pulse is used to acquire the central k_x segment every time.

This study describes an extension of this reacquisition technique to 2D navigator sequences, in which the navigator data are used during the scan to identify and resample data that cannot be corrected by 2D nonlinear phase correction. It is demonstrated that this 2D-navigator-based reacquisition scheme can be combined with readout-segmented EPI and parallel imaging to provide a robust method for high resolution diffusion-weighted imaging, which has a low level of image distortion and is insensitive to motion-induced phase error. A preliminary account of this work has been presented elsewhere (25,26). Also note that subsequent clinical application of diffusion-weighted (DW) readout-segmented EPI with GRAPPA (GeneRalized Autocalibrating Partially Parallel Acquisitions) has also shown promising results in other studies (27).

THEORY AND METHODS

Readout-Segmented EPI

The readout-segmented EPI sequence used in this study is shown schematically in Figure 1. After a diffusion preparation, two spin echoes were used to acquire imaging and navigator data, respectively, using a sinusoidal EPI readout, which sampled a subset of contiguous points in the readout direction. For the first spin echo, a variable amplitude prephasing pulse (colored blue in Fig. 1) was applied to define an offset along k_x, which was varied from one shot to the next. In this manner, each shot was used to sample a different segment in the k_x direction (see Fig. 2). The smaller readout gradient moment, corresponding to the reduced k_x coverage, allows a substantially shorter

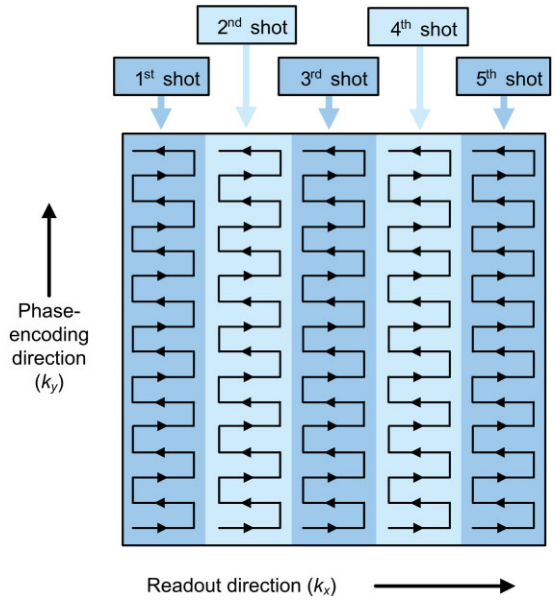

FIG. 2. Depiction of the *k*-space coverage for readout segmented EPI. In this example, a five-shot EPI acquisition is used, which divides *k*-space into five segments along the readout direction. Each shot acquires data from a set of contiguous *k*-space sample points, which is beneficial for 2D navigator phase correction. In practice, a small overlap is used at the interface between readout segments (see main text). [Color figure can be viewed in the online issue, which is available at www.interscience.wiley.com.]

echo-spacing than with single-shot EPI, significantly reducing the effect of susceptibility and T_2^* decay. The second echo was used to generate 2D navigator data by sampling the central k_x segment at each shot. A blipped phase-encoding gradient was used to traverse the full k_y range.

A small overlap was used between the individual readout segments, which for clarity is not shown in Figure 2. This overlap serves two purposes. The first purpose relates to the regridding required for the sinusoidal readout gradient waveform. By sampling additional k_x points at the start and end of each readout, the regridded k_x points that correspond to the actual interface between readout segments can be more precisely determined by including the contribution from these additional points in the convolution process used during regridding. It is critical that a precise regridding process is applied to avoid a mismatch at the interface between the readout segments. The second purpose for the overlap concerns the 2D navigator correction and is addressed in detail below. For the images acquired in this study a fixed overlap of eight k_x sample points was used, so that four additional data points were sampled at the start and end of each readout.

With readout-segmented EPI it is essential that the *k*-space trajectory along k_x is carefully controlled so that there are no discontinuities at the interface between readout segments, which can cause ghosting in the final image. This places some strict requirements on the data sampling and gradient hardware, which may not always be fulfilled. In particular, the readout gradient moment sampled at each echo in the EPI echo-train must be consistent with the increments used for the readout prephasing pulse (colored blue in Fig. 1). Small discrepancies can arise between these two gradients if there is a temporal displacement between the data sampling window and the applied readout gradient or if the actual readout gradient waveform deviates from the ideal case. During the current work, the time-shift problem was overcome by using a predetermined gradient delay and applying a standard first-order phase correction along the k_x dimension of the raw data using non–phase-encoding reference data. In addition, to correct the readout gradient moment arising from deviations of the waveform from the ideal sinusoidal shape, the gradient amplitude was manually adjusted to ensure optimum image quality. This was achieved by acquiring a set of phantom images with gradient amplitude scaling factors in the range 0.98 to 1.02. A visual inspection of the images was then used to select the optimum scaling factor, corresponding to the image with minimum ringing artifact in the readout direction. Typically, this optimum scaling factor represented a change in gradient amplitude of less than 1% compared with the nominal value. This optimum scaling factor was then used to scale the readout gradients during the subsequent acquisition of images in vivo.

The readout-segmented EPI technique was combined with parallel imaging by undersampling *k*-space in the k_y direction during both imaging and navigator echo-trains. This provides a further reduction in susceptibility and T_2^* decay artifacts by shortening the EPI echo-train length and decreasing the effective echo-spacing. The GRAPPA method (28) was used to reconstruct the undersampled data, for which the autocalibration signals (ACS) were acquired using a single-shot EPI readout that sampled data from the central region of *k*-space in both k_x and k_y directions.

2D-Navigator-Based Reacquisition

During the measurement, a reacquisition process was used to repeat scans that resulted in unusable data. These unusable data sets are characterized by navigator images with a large nonlinear phase error, which corresponds to a broadening of the signal distribution in *k*-space. This *k*-space broadening was used to identify the affected scans directly from the *k*-space data by using the width of the signal distribution in the k_x direction as a measure for the extent of the nonlinear phase error.

This distribution width, W_x, was characterized using the following expression for the first moment of the signal distribution along the k_x direction:

$$W_x = \sum_i \sum_{k_y} \sum_{k_x} |S_i(k_x,k_y)| \cdot |k_x - \Omega_x| \qquad [1]$$

where the summation is performed over the set of sampled *k*-space points in the 2D navigator for each receive coil *i*, S_i is the complex *k*-space signal for each receive coil and Ω_x is the k_x coordinate corresponding to the maximum signal amplitude when summed across all receive channels (this is taken to represent the centre of the signal distribution). Note that this expression is particularly convenient for parallel imaging applications, as it can be applied directly to undersampled data sets without any further processing. This makes it suitable for the real-time calculations that are required during the reacquisition process.

The reacquisition was performed at the end of the standard measurement when all readout segments had been scanned for all b-values and diffusion-encoding directions. During reacquisition an independent decision about which scans to reacquire was made for each slice position. The first step in this decision-making process was to compare all shots for a given image (i.e., for a given b-value and diffusion direction) and identify the segment with the smallest distribution width W_x. This width was then used as a reference point for all other readout segments for that image and in each case a relative distribution width was calculated. Segments with relative widths exceeding an empirical threshold of 1.05 times the reference width were marked for reacquisition. This process was repeated for all images to identify the complete set of scans to be reacquired. The order of the reacquisitions was weighted toward data sets with large relative distribution widths but, similar to the approach taken in previous work (23), an increased weighting was also given to readout segments closest to the centre of *k*-space, where corrupt data has a greater influence on image quality. In addition, an overall time limit was placed on the time spent reacquiring data, which was set to 20% of the standard measurement time.

Image Reconstruction

After using a standard regridding procedure (29) along the k_x direction to compensate for the sinusoidal readout gradient waveform, Nyquist ghost phase correction was performed using reference data from a non–phase-encoded EPI echo-train. An adapted GRAPPA reconstruction was then applied to the regridded, Cartesian sampled data from each readout segment to reconstruct the missing k_y data points. For this GRAPPA reconstruction, the coil weights were derived from the ACS data using a Moore-Penrose pseudo inverse and a 2D convolution kernel (30) was used with four source points along the phase-encoding direction and three source points along the readout direction. The same processing was applied to both imaging and navigator data, yielding in each case a separate *k*-space data set for each receive channel.

2D nonlinear navigator phase correction was then applied independently to the data from each readout segment and receive channel as follows. The imaging data were zero-filled and Fourier transformed to provide a complex image domain data set. In a similar way, the corresponding 2D navigator data were also transformed to the image domain, although in this case a *k*-space Hanning filter was applied in the k_x direction to minimize truncation artifacts. The navigator data were then normalized and used to phase correct the imaging data by performing a pixel by pixel complex multiplication. Although the image domain data from an individual readout segment only represent a subset of the spatial frequencies required for the final image, this image domain phase correction procedure is not corrupted by aliased signal contributions because the sampled points are contiguous in *k*-space, thereby fulfilling the Nyquist sampling condition for the specified FOV.

One important point to consider in relation to this phase correction procedure is the effect of the limited number of k_x points in the segment of data being corrected. The nonlinear, image-domain phase correction corresponds to a redistribution of the raw data signals in *k*-space, in which signals from some regions of the object are shifted by more than those from other regions, according to the local motion-induced phase variations. Due to this *k*-space redistribution, a potential problem arises at the edge of the readout segment when the effect of the phase correction is to try to recover data that have been shifted outside the segment. These data are of course not available because they fall outside the sampled region, thereby limiting the effectiveness of the phase correction. This provides a further motivation for sampling additional k_x points at the start and end of each readout event. This has the effect of making the sampled region wider in the k_x direction than required, so that shifted signals at the edge of the readout segment can be recovered. Note also that the zero-filling in the k_x direction at the start of the phase-correction procedure is necessary to avoid aliasing in *k*-space when the image-domain phase correction shifts *k*-space signals outside of the sampled region.

After navigator phase correction, the data were transformed back to *k*-space and the additional readout columns at the edge of each segment were discarded. The data from all readout segments were then combined, before applying a final transformation back into the image domain to produce a separate image for each receive channel. Image data from all receive channels were then combined in a standard way using the square root of the sum of squares.

Imaging Experiments

The readout-segmented EPI sequence with 2D navigator-based reacquisition was implemented on a 1.5T MAGNETOM Avanto system and a 3T MAGNETOM Trio system (Siemens Healthcare, Erlangen, Germany). For protocols without parallel imaging, image reconstruction was performed on the scanner using a modified reconstruction program and for protocols with parallel imaging, the reconstruction was performed off-line using MATLAB (The Mathworks Inc., Natick, MA). All studies were performed on healthy volunteers without cardiac triggering using standard 12-channel head coils. Informed consent was obtained from all subjects before each study.

At 1.5T, readout-segmented EPI images were acquired with the following parameters: no parallel imaging, FOV 230 mm, matrix 224 × 224, pixel size 1.0 mm × 1.0 mm, slices 17, slice thickness 5 mm, number of readout segments per image 11, echo-spacing 300 μs, TR 3860 ms, echo time (TE) 82 ms, one scan at b = 0 s/mm^2 and three at b = 1000 s/mm^2 in orthogonal directions, one average, total measurement time (including reacquisitions, a Nyquist ghost phase-correction scan and a dummy scan for magnetization preparation) 3 min 25 s.

At 3T, readout-segmented EPI images were acquired with the following parameters: parallel imaging using GRAPPA with an acceleration factor of 2, FOV 210 mm, matrix 224 × 224, pixel size 0.9 mm × 0.9 mm, slices 19, slice thickness 5 mm, number of readout segments per image 11, echo-spacing 320 μs, TR 3380 ms, TE 68 ms, one scan at b = 0 s/mm^2 and three at b = 1000 s/mm^2 in orthogonal directions, one average, total measurement

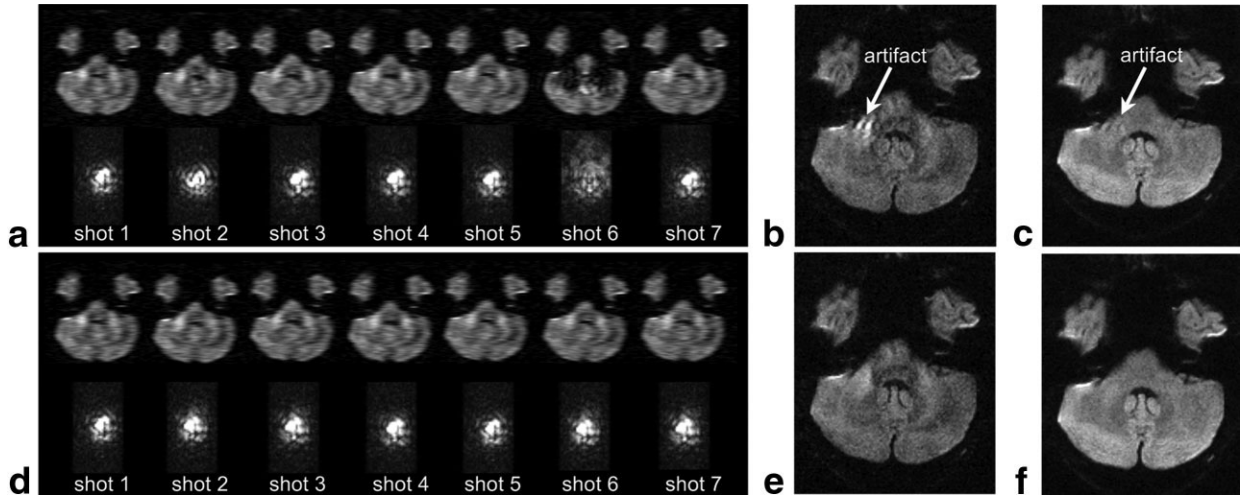

FIG. 3. Example showing the effect of the 2D navigator based reacquisition. **a:** The navigator data from the central seven shots of a diffusion-weighted data set before data reacquisition. Top row: low resolution navigator images; bottom row: corresponding *k*-space data. Shot 6 has a signal void artifact in the navigator image, which is seen as a widened signal distribution in *k*-space. **b,c:** The corresponding artifact in the reconstructed diffusion- and trace-weighted images, respectively. **d:** The navigator data after reacquisition. Data sets with wide *k*-space signal distributions have been replaced by newly acquired data. **e,f:** The corresponding artifact-free images reconstructed using the reacquired data.

time (including reacquisitions, a Nyquist ghost phase-correction scan, a GRAPPA auto-calibration scan and a dummy scan for magnetization preparation) 3 min 6 s.

At 3T, standard DW single-shot EPI images were also acquired for comparison using the following parameters: parallel imaging using GRAPPA with an acceleration factor of 2, FOV 230 mm, matrix 192 × 192, phase partial Fourier factor 6/8, pixel size 1.2 mm × 1.2 mm, slices 19, slice thickness 5 mm, echo-spacing 900 μs, TR 2800 ms, TE 87 ms, one scan at b = 0 s/mm^2 and three at b = 1000 s/mm^2 in orthogonal directions, four averages, total measurement time (including a GRAPPA autocalibration scan and a dummy scan for magnetization preparation) 50 s.

RESULTS

Figure 3 shows data from a 1.5T examination, which illustrates the effectiveness of the reacquisition procedure for an imaging slice at the base of the brain. The top row of Figure 3a shows the low-resolution navigator images corresponding to the central seven readout segments (or shots) of the standard measurement before data reacquisition. The corresponding *k*-space data in modulus format are shown in the second row of Figure 3a. With the exception of shot number six, the navigator images and corresponding *k*-space signal distributions are very similar. The navigator image from shot six, however, has bilateral signal voids in the anterior part of the cerebellum with a corresponding wide signal distribution in *k*-space. The effect of these corrupt data is to produce a localized artifact in the final reconstructed image as shown in Figure 3b. The artifact is most noticeable on the right side of the brain in the region indicated by the arrow in the figure. Similarly, Figure 3c shows the effect of the corrupt data when the image from Figure 3b is used to produce a trace-weighted image (by taking the geometric mean of the three DW images with mutually orthogonal diffusion-encoding directions).

Figure 3d shows the corresponding set of navigator images after the automatic data reacquisition procedure, which consisted of 7 reacquisitions, requiring an additional 27 s of measurement time. The readout segments with relatively large *k*-space signal distributions have been reacquired, which is most noticeable with shot number six. As shown in Figure 3d,e, the modified data produce images without the artifact seen with the standard data set. The trace-weighted image in Figure 3e demonstrates that the readout-segmented EPI method can provide good quality diffusion-weighted images at 1.5T with low susceptibility artifact. Note that these images were acquired without parallel imaging, which would provide a further reduction in susceptibility and T_2^* decay effects.

Figures 4 and 5 provide a comparison between readout-segmented EPI and single-shot EPI at 3T. In both figures, the top row shows the single-shot EPI images, acquired using a GRAPPA acceleration factor of 2, and the bottom rows show the corresponding high-resolution readout-segmented EPI images, also acquired using a GRAPPA acceleration factor of 2. In this case, the automatic reacquisition procedure resulted in eight reacquisitions, corresponding to an additional 27 s of measurement time. In both figures, the left column shows images with a nominal b-value of zero and the right column shows trace-weighted images with a nominal b-value of 1000 s/mm^2. Figure 4 shows comparative images for a slice position at the base of the brain, where susceptibility artifacts are generally at their most severe. This region is also particularly challenging for multishot DW imaging due to the high level of CSF pulsation around this part of the brain, leading to large nonlinear phase errors. The readout-segmented EPI data show a substantial reduction in susceptibility artifact and anatomical detail compared with the single-shot images

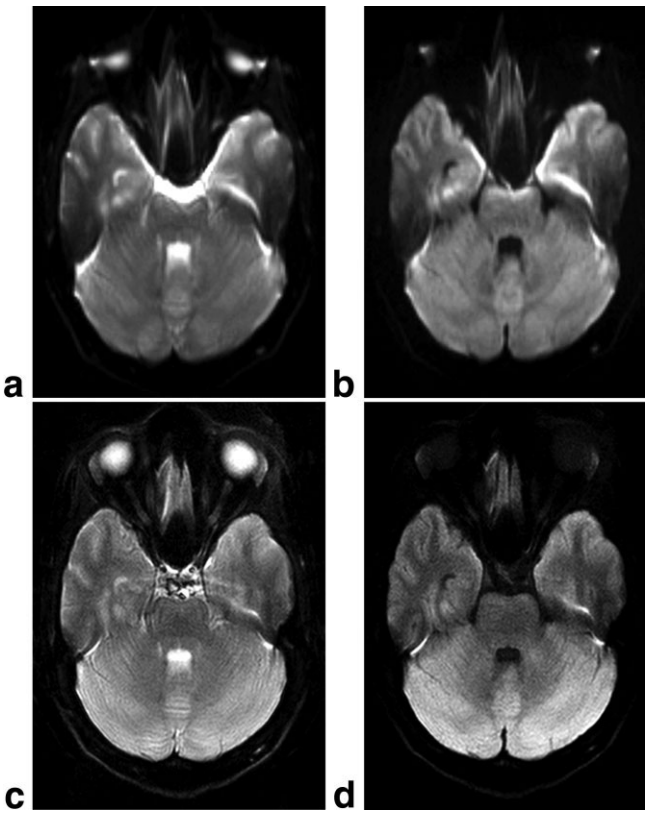

FIG. 4. Direct comparison between single-shot EPI and readout segmented EPI at the base of the brain. **a,b:** Single-shot EPI acquisition with b = 0 s/mm^2 (a) and corresponding trace-weighted image with b = 1000 s/mm^2 (b). **c,d:** Readout segmented EPI with b = 0 s/mm^2 (c) and corresponding trace-weighted image with b = 1000 s/mm^2 (d)

and without any evidence of residual motion-induced phase error. Similarly, Figure 5d shows typical artifact-free images for an axial slice at the level of the lateral ventricles, a region that is also affected by CSF pulsation. Although single-shot EPI images at this slice position do not exhibit a marked susceptibility artifact, the readout-segmented EPI images still demonstrate a higher image quality due to the substantial improvement in anatomical detail.

DISCUSSION

As seen in Figure 4, standard single-shot EPI protocols are prone to significant susceptibility artifact at 3T, even when parallel imaging techniques, such as GRAPPA, are used to reduce the effective echo-spacing. In addition, although parallel imaging has made it possible to increase the resolution that can be achieved with single-shot EPI, by reducing the length of the echo-train for a given *k*-space coverage, the resolution is still limited compared with other MR imaging methods. This resolution limitation is imposed by the T_2^* decay during the echo-train, which results in a blurring of the signal in the phase-encoding direction and sets a practical limit on the length of echo-train that can be used for data acquisition. Furthermore, because T_2^* values reduce with increasing field strength, this blurring effect is more significant at 3T than at 1.5T, making it more difficult to achieve a high-resolution with single-shot EPI.

The readout-segmented EPI method significantly reduces these limitations by allowing a shorter echo-spacing in the EPI echo-train compared with the single-shot case due to the smaller number of k_x points that are sampled during each readout gradient. The method is easily combined with GRAPPA, using the same methodology as that developed for single-shot EPI, resulting in an effective echo-spacing that is many times shorter than that of the equivalent single-shot EPI scan with the same resolution. Taking the GRAPPA acceleration factor of 2 into account, the readout-segmented EPI images in Figures 4 and 5, correspond to an effective echo-spacing of 160 μs, whereas an equivalent single-shot EPI protocol with GRAPPA would have had an effective echo-spacing of around 700 μs. In the case of the comparison shown in Figure 4, the single-shot EPI scan still had a significantly longer effective echo-spacing (450 μs) despite the lower resolution. Furthermore, for the single-shot EPI measurement there was a time period of 43.2 ms between the acquisition of the central *k*-space echo and the end of the echo-train, where the outer k_y line was sampled. The equivalent time period of 17.9 ms for the readout-segmented EPI sequence was much shorter despite the larger *k*-space coverage. Consequently, the improvement in the anatomical detail seen in the readout-segmented EPI images of Figures 4 and 5 is

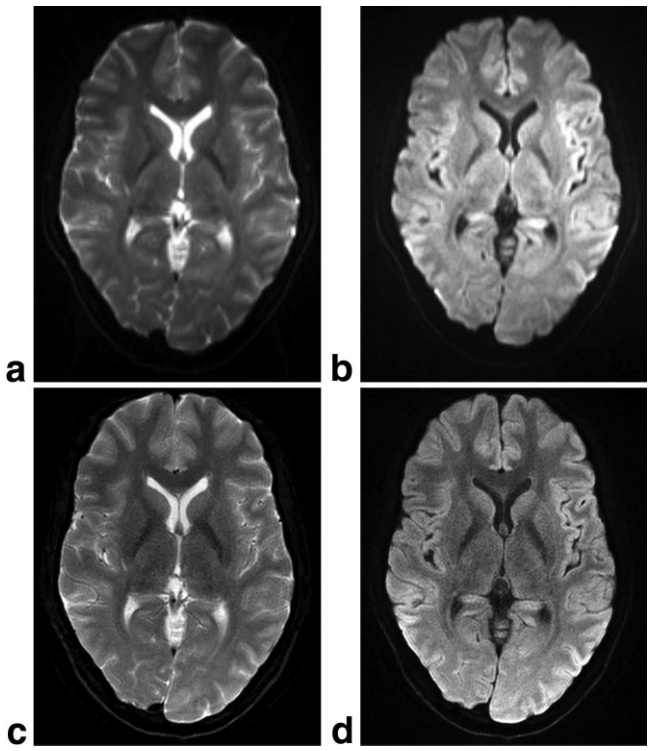

FIG. 5. Direct comparison between single-shot EPI and readout segmented EPI in the brain at the level of the lateral ventricles. **a,b:** Single-shot EPI acquisition with b = 0 s/mm^2 (a) and corresponding trace-weighted image with b = 1000 s/mm^2 (b). **c,d:** Readout segmented EPI with b = 0 s/mm^2 (c) and corresponding trace-weighted image with b = 1000 s/mm^2 (d).

attributable both to the higher nominal resolution and to a reduction in T_2^* blurring effects.

The implementation of readout-segmented EPI described in this study did not use partial Fourier in the phase-encoding direction, as is typically the case with single-shot EPI protocols, including those used in the current work. Although this would also be an option for the readout-segmented EPI technique, the reduction in TE would be less significant than with single-shot EPI due to the shorter echo-train. Consequently, it might be preferable to use a full *k*-space acquisition along k_y and avoid some of the difficulties that are associated with the reconstruction of phase partial Fourier diffusion-weighted EPI data, leading to artifact or loss of spatial resolution (31). Another advantage to using a full k_y acquisition, which could be explored in future work, is that it may allow some of the readout segments on one side of *k*-space to be omitted from the acquisition and a partial Fourier reconstruction used for the k_x direction. This would have the benefit of decreasing the number of spin excitations required for a given image resolution, which would be useful for scan time reduction, particularly if the technique were used to scan multiple diffusion directions in a DTI study.

This study has demonstrated that the readout-segmented EPI acquisition scheme can be combined with a simple image-based complex multiplication to provide a robust correction for the nonlinear phase errors that arise from subject motion in diffusion-weighted imaging. Compared with acquisition schemes that do not sample contiguous *k*-space sample points, there is a considerable reduction in computational effort during image reconstruction, as there is no requirement for an iterative phase correction procedure.

All imaging techniques, which rely on 2D navigator phase correction will fail when the spatial frequency of the motion-induced phase errors becomes too large. As illustrated by the data shown in Figure 3, the incidence of these highly corrupt data sets is quite low for diffusion-weighted imaging of the brain, affecting particular brain regions at certain points in the cardiac cycle. This makes it possible to avoid the corresponding image artifacts by reacquiring a small subset of scans, which are identified as unusable in real time during the acquisition. A measure of the relative width of the *k*-space signal distribution has been shown by this study to be an effective way of controlling this reacquisition process. The procedure adopted in this work used a relative width threshold of 1.05 and restricted the maximum time spent reacquiring data to 20% of the standard measurement time. In preliminary measurements, this approach was found to be sufficient to avoid the occasional artifacts that otherwise occur. To ensure a good compromise between scan time and artifact suppression, further work with a large number of subjects is required to fully optimize these two criteria used to determine the number of reacquisitions in a range of measurement protocols.

A recent clinical application of the DW segmented EPI method (27) acquired images with an implementation of the sequence that did not include the navigator-controlled reacquisition. To compensate for this, these acquisitions used a very large overlap between readout segments, corresponding to as much as 50% of the width of the segment, making it possible to correct for large *k*-space signal displacements. A disadvantage to this approach is that a substantial increase in the overlap region is required to accommodate the kind of *k*-space distribution seen in the navigator data of shot number 6 in Figure 3. The resulting increase in the width of the readout segments leads, in turn, to a significant increase in the echo-spacing and TE compared with a reacquisition strategy, in which these infrequent, highly corrupt data sets are discarded. Nevertheless, this approach may be a useful option in the absence of real-time feedback between data analysis and data acquisition.

There are two further outstanding issues that affect the routine application of DW readout-segmented EPI. The first of these is the manual adjustment used in this work to scale the readout gradient to ensure *k*-space continuity at the interfaces between readout segments. As seen in the images of Figures 3–5, this adjustment procedure is effective at avoiding ringing artifact in the subsequent images acquired in vivo. However, this process will need to be automated for routine use, so that adjustment parameters can be easily established for a wide range of measurement protocols. This could be done either by using an automated version of the adjustment process described above, or by leaving the readout amplitude fixed and using information from a *k*-space trajectory measurement to re-grid the data along k_x (32). In this latter approach the additional k_x points, sampled at the edges of readout segments, would allow the effective moment of the readout gradient to be increased if required.

The second outstanding issue is that of rigid-body motion. The 2D image-domain phase correction used in the current work addresses the problem of motion during the diffusion preparation, but not the problem of rigid-body motion between the acquisition of different readout segments, which leads to a loss of detail in the final image due to misregistration of the data. In future work, this rigid-body problem could be addressed by performing an image registration of the navigator images from different shots and using the information to realign the data from the individual readout segments. This could be achieved using techniques derived from motion correction procedures described elsewhere, such as those used with the self-navigated PROPELLER sequence (33).

CONCLUSION

This study has described a new multishot technique for acquiring high-resolution DW images, which have low susceptibility based image distortion and T_2^* blurring and a robust correction for motion-induced phase artifact. The technique provides significant image quality improvement compared with DW single-shot EPI at 3T with relatively short scan times, making the technique of interest for DWI and DTI in routine clinical studies.

REFERENCES

1. Warach S, Gaa J, Siewert B, Wielopolski P, Edelman RR. Acute human stroke studied by whole brain echo planar diffusion-weighted magnetic resonance imaging. Ann Neurol 1995;37:231–241.

2. van Everdingen KJ, van der Grond J, Kappelle LJ, Ramos LM, Mali WP. Diffusion-weighted magnetic resonance imaging in acute stroke. Stroke 1998;29:1783–1790.
3. Wu O, Koroshetz WJ, Ostergaard L, Buonanno FS, Copen WA, Gonzalez RG, Rordorf G, Rosen BR, Schwamm LH, Weisskoff RM, Sorensen AG. Predicting tissue outcome in acute human cerebral ischemia using combined diffusion- and perfusion-weighted MR imaging. Stroke 2001; 32:933–942.
4. Turner R, Le Bihan D, Maier J, Vavrek R, Hedges LK, Pekar J. Echo-planar imaging of intravoxel incoherent motion. Radiology 1990;177: 407–414.
5. Griswold MA, Jakob PM, Chen Q, Goldfarb J, Manning WJ, Edelman RR, Sodickson DK. Resolution enhancement in single-shot imaging using simultaneous acquisition of spatial harmonics (SMASH). Magn Reson Med 1999;41:1236–1245.
6. Griswold MA, Jakob PM, Heidemann RM, Nittka M, Wang J, Kiefer B, Haase. A Off-resonance artifacts in single shot EPI using partially parallel imaging. In: Proceedings of the 9th Annual Meeting of ISMRM, Glasgow, Scotland, 2001. (abstract 446).
7. Heidemann RM, Griswold MA, Porter D, Kiefer B, Nittka M, Wang J, Haase A, Jakob PM. Minimizing distortions and blurring in diffusion weighted single shot EPI using high performance gradients in combination with parallel imaging. In: Proceedings of the 9th Annual Meeting of ISMRM, Glasgow, Scotland, 2001. (abstract 169).
8. Bammer R, Keeling SL, Augustin M, Pruessmann KP, Wolf R, Stollberger R, Hartung HP, Fazekas F. Improved diffusion-weighted single-shot echo-planar imaging (EPI) in stroke using sensitivity encoding (SENSE). Magn Reson Med 2001;46:548–554.
9. Ordidge RJ, Helpern JA, Qing ZX, Knight RA, Nagesh V. Correction of motional artefacts in diffusion-weighted MR images using navigator echoes. Magn Reson Imaging 1994;12:455–460.
10. Anderson AW, Gore JC. Analysis and correction of motion artifacts in diffusion weighted imaging. Magn Reson Med 1994;32:379–387.
11. Miller KL, Pauly JP. Nonlinear phase correction for navigated diffusion imaging. Magn Reson Med 2003;50:343–353.
12. Butts K, Pauly J, de Crespigny A, Moseley M. Isotropic diffusion-weighted and spiral-navigated interleaved EPI for routine imaging of acute stroke. Magn Reson Med 1997;38:741–749.
13. Atkinson D, Porter DA, Hill DLG, Calamante F, Connelly A. Sampling and reconstruction effects due to motion in diffusion-weighted interleaved echo-planar imaging. Magn Reson Med 2000;44:101–109.
14. Liu C, Bammer R, Kim D, Moseley ME. Self-navigated interleaved spiral (SNAILS): application to high-resolution diffusion tensor imaging. Magn Reson Med 2004;52:1388–1396.
15. Atkinson D, Counsell S, Hajnal JV, Batchelor PG, Hill DL, Larkman DJ. Nonlinear phase correction of navigated multi-coil diffusion images. Magn Reson Med 2006;56:1135–1139.
16. Pipe JG, Farthing VG, Forbes KP. Multishot diffusion-weighted FSE using PROPELLER MRI. Magn Reson Med 2002;47:42–52.
17. Liu G, van Gelderon P, Duyn J, Moonen CTW. Single-shot diffusion MRI of human brain on a conventional clinical instrument. Magn Reson Med 1996;35:671–677.
18. Wang F-N, Huang T-Y, Lin F-H, Chuang T-C, Chen N-K, Chung H-W, Chen C-Y, Kwong KK. PROPELLER EPI: an MRI technique suitable for diffusion tensor imaging at high field strength with reduced geometric distortions. Magn Reson Med 2005;54:1232–1240.
19. Robson MD, Anderson AW, Gore JC. Diffusion-weighted multiple-shot echo planar imaging of humans without navigation. Magn Reson Med 1997;38:82–88.
20. Porter DA, Mueller E. Multi-shot diffusion-weighted EPI with readout mosaic segmentation and 2D navigator correction. In: Proceedings of the 12th Annual Meeting of ISMRM, Kyoto, Japan, 2004. (abstract 442).
21. Wirestam R, Greitz D, Thomsen C, Brockstedt S, Olsson MB, Stahlberg F. Theoretical and experimental evaluation of phase-dispersion effects caused by brain motion in diffusion and perfusion MR imaging. J Magn Reson Imaging 1996;6:348–355.
22. Nunes RG, Jezzard P, Clare S. Investigations on the efficiency of cardiac-gated methods for the acquisition of diffusion-weighted images. J Magn Reson 2005;177:102–110.
23. Nguyen Q, Clemence M, Ordidge RJ. The use of intelligent re-acquisition to reduce scan time in MRI degraded by motion. In: Proceedings of the 6th Annual Meeting of ISMRM, Sydney, Australia, 1998. (abstract 134).
24. Nguyen Q, Clemence M, Thornton J, Ordidge RJ. Isotropic diffusion-weighted multishot imaging using automatic reacquisition. In: Proceedings of the 7th Annual Meeting of ISMRM, Philadelphia, Pennsylvania, USA, 1999. (abstract 559).
25. Porter DA, Heidemann RM. Multi-shot, diffusion-weighted imaging at 3T using readout-segmented EPI and GRAPPA. In: Proceedings of the 14th Annual Meeting of ISMRM, Seattle, Washington, USA, 2006. (abstract 1046).
26. Porter DA. 2D-navigator-based re-acquisition for motion artefact suppression in multi-shot, diffusion-weighted imaging. In: Proceedings of the 14th Annual Meeting of ISMRM, Seattle, Washington, USA, 2006. (abstract 1047).
27. Holdsworth SJ, Skare S, Newbould RD, Guzmann R, Blevins NH, Bammer R. Readout-segmented EPI for rapid high resolution imaging at 3T. Eur J Radiol 2008;65:36–46.
28. Griswold MA, Jakob PM, Heidemann RM, Nittka M, Jellus V, Wang J, Kiefer B, Haase A. Generalized autocalibrating partially parallel acquisitions (GRAPPA). Magn Reson Med 2002;47:1202–1210.
29. Jackson JI, Meyer CH, Nishimura DG, Macovski A. Selection of a convolution function for Fourier inversion using gridding. IEEE Trans Med Imaging 1991;10:473–478.
30. Griswold MA. Advanced *k*-space techniques. In: Proceedings of the 2nd International Workshop on Parallel MRI, Zurich, Switzerland, 2004. p 16–18.
31. Robson MD, Porter DA. Reconstruction as a source of artifact in non-gated single-shot diffusion-weighted EPI. Magn Reson Imaging 2005; 23:899–905.
32. Josephs O, Deichmann R, Turner R. Trajectory Measurement and Generalised Reconstruction in Rectilinear EPI. In: Proceedings of the 8th Annual Meeting of ISMRM, Denver, Colorado, USA, 2000. (abstract 1517).
33. Pipe J. Motion correction with PROPELLER MRI: application to head motion and free-breathing cardiac imaging. Magn Reson Med 1999;42: 963–969.